Published December 8, 2014

Thromboxane A2 acts as tonic immunoregulator by preferential disruption of low-avidity CD4+ T cell–dendritic cell interactions

Federica Moalli,[1] Jovana Cupovic,[2] Flavian Thelen,[1] Pascal Halbherr,[1] Yoshinori Fukui,[3,4] Shuh Narumiya,[5] Burkhard Ludewig,[2] and Jens V. Stein[1]

[1]Theodor Kocher Institute, University of Bern, 3012 Bern, Switzerland
[2]Institute of Immunobiology, Cantonal Hospital St. Gallen, CH-9007 St. Gallen, Switzerland
[3]Division of Immunogenetics, Department of Immunobiology and Neuroscience, Medical Institute of Bioregulation and
[4]Research Center for Advanced Immunology, Kyushu University, Fukuoka 812-8582, Japan
[5]Department of Pharmacology, Faculty of Pharmaceutical Sciences, Kyoto University, Kyoto 606-8501, Japan

Interactions between dendritic cells (DCs) and T cells control the decision between activation and tolerance induction. Thromboxane A2 (TXA2) and its receptor TP have been suggested to regulate adaptive immune responses through control of T cell–DC interactions. Here, we show that this control is achieved by selectively reducing expansion of low-avidity CD4+ T cells. During inflammation, weak tetramer-binding TP-deficient CD4+ T cells were preferentially expanded compared with TP-proficient CD4+ T cells. Using intravital imaging of cellular interactions in reactive peripheral lymph nodes (PLNs), we found that TXA2 led to disruption of low- but not high-avidity interactions between DCs and CD4+ T cells. Lack of TP correlated with higher expression of activation markers on stimulated CD4+ T cells and with augmented accumulation of follicular helper T cells (T_{FH}), which correlated with increased low-avidity IgG responses. In sum, our data suggest that tonic suppression of weak CD4+ T cell–DC interactions by TXA2–TP signaling improves the overall quality of adaptive immune responses.

CORRESPONDENCE
Jens V. Stein:
jstein@tki.unibe.ch

Abbreviations used: 2PM, two-photon microscopy; APL, altered peptide ligand; LCMV, lymphocytic choriomeningitis virus; MC, motility coefficient; mLN, mesenteric LN; pMHC, peptide MHC; PLN, peripheral LN; T_{FH}, helper T cell; TXA2, Thromboxane A2.

T cells have evolved to quickly react to potentially dangerous microbes by recognizing pathogen-derived peptide (p)-MHC complexes displayed on antigen-presenting cells, in particular DCs. Because T cells are selected in the thymus for their ability to recognize self-pMHC complexes (Morris and Allen, 2012) and numerous self-reactive T cells are released into the periphery (Su et al., 2013), peripheral tolerance education is critical to avoid activation of autoreactive T cells. Studies using intravital two-photon microscopy (2PM) of reactive PLNs have shed light on the dynamic T cell–DC interactions and their correlation with full versus curtailed T cell activation and tolerance induction. The amount of cognate pMHC complexes on activated DCs is critical in determining the transition of a highly motile scanning-mode T cell to an immotile, stably interacting one (Cahalan and Parker, 2006; Henrickson and von Andrian, 2007; Bajénoff and Germain, 2007). Such stable T cell–DC interactions (>8h) are a prerequisite for full effector T cell differentiation (Rachmilewitz and Lanzavecchia, 2002). Thus, in presence of high amounts of cognate pMHC on activated DCs, T cells decelerate rapidly, whereas T cells show a motile DC sampling behavior when cognate pMHC levels are low. Altered peptide ligands (APLs) with reduced affinity for a given TCR also decrease the length of T cell–DC interactions, limiting T cell activation. Under tolerogenic conditions (i.e., in the absence of co-stimulation), 2PM studies uncovered shortened T cell–DC interactions (Hugues et al., 2004) although this is still controversial (Shakhar et al., 2005). Similarly, the presence of regulatory T (T reg) cells reduces

Published December 8, 2014

T cell–DC interactions and subsequent T cell activation (Tadokoro et al., 2006; Tang et al., 2006).

A perhaps counterintuitive recent finding has revealed a significant increase in $CD8^+$ T cell immune response avidity in presence of T reg cells (Pace et al., 2012). This is due to T reg cell–mediated suppression of excessive interactions between DCs and $CD8^+$ T cells bearing TCRs with low avidity for pMHC complexes. In the absence of T reg cells, uncontrolled CCR5 ligand secretion by activated DCs induces attraction of bystander TCR clones with low affinity for pMHC complexes, which decreases overall avidity and memory T cell generation of the resulting immune response. Whether a comparable mechanism also exists to selectively support activation of high avidity $CD4^+$ T cells by immunoregulatory factors is currently unknown.

The short-lived arachidonic acid–derived lipid thromboxane A2 (TXA2) has been suggested to regulate adaptive immune responses (Kabashima et al., 2003). Activated DCs and other cell types produce TXA2, which binds its G-protein coupled receptor TP expressed in thymocytes and naive but not effector/memory $CD4^+$ and $CD8^+$ T cells. Addition of high amounts of the TP agonist I-BOP induces chemokinesis in naive T cells and decreases in vitro aggregate formation between T cells and DCs, causing reduced T cell activation (Kabashima et al., 2003). Combined with the observation that TXA2 levels rapidly rise in reactive PLN during immune responses (Moore et al., 1989), these data suggest a model where TXA2 may act as a general suppressor of T cell–DC interactions. In line with this hypothesis, aged TP-deficient T cells develop lymphoid hyperplasia and high antibody titers (Kabashima et al., 2003). Yet, it has remained unknown how TXA2 signaling affects dynamic $CD4^+$ T cell interactions with DC displaying varying pMHC abundance and affinity in vivo, and how this impacts avidity patterns of responding T cells.

Here, we show that during sterile and microbial inflammation, absence of TP resulted in increased expansion of low-avidity $CD4^+$ T cells. Using 2PM imaging of cellular interactions in reactive PLNs, we report that paracrine TXA2 signaling preferentially disrupted low-avidity interactions between DCs and OT-II $CD4^+$ T cells induced by low cognate pMHC levels or low-affinity peptide. As a consequence, $TP^{-/-}$ OT-II $CD4^+$ T cells show increased expression of early activation markers, as well as augmented accumulation of follicular helper T cells (T_{FH}) compared with WT OT-II $CD4^+$ cells. High numbers of $TP^{-/-}$ T_{FH} correlated with increased low-avidity IgG production, thus thwarting the overall quality of the adaptive immune response. In sum, our data uncover a previously unappreciated contribution of a tolerance-inducing mechanism for preferential activation of high avidity $CD4^+$ T cells.

RESULTS AND DISCUSSION

Lack of TP lowers overall polyclonal $CD4^+$ T cell avidity during inflammation

$TP^{-/-}$ mice were reported to develop lymphadenopathy and increasing circulating Ig levels with age (>26 wk; Kabashima et al., 2003). In our SPF colony, we observed enlarged mesenteric LNs (MLNs), occasionally accompanied by splenomegaly, in $TP^{-/-}$ mice >3 mo old (unpublished data). We therefore evaluated antigen-specific adaptive immune responses in younger WT and $TP^{-/-}$ mice (5–8 wk), which displayed normal lymphoid organ size and showed no signs of spontaneous lymphocyte activation (unpublished data). Because physiological T cell responses involve low- and high-avidity TCR T cells (Sabatino et al., 2011), we examined the role of TP during expansion of Ag-specific $CD4^+$ T cells recognizing OVA-derived peptides after s.c. OVA/CFA immunization (Fig. S1 A). Both WT and $TP^{-/-}$ mice showed expansion of low- and high-avidity OVA-peptide tetramer-positive (OVA tet^+) $CD4^+$ T cells on day 8 after immunization in draining PLNs (Fig. 1 A). Notably, we found a larger increase of OVA tet^+ $CD4^+$ T cells in reactive PLNs of $TP^{-/-}$ mice as compared with WT mice (Fig. S1 B), in particular among the weak-binding OVA tet^+ low population (Fig. 1 B). When we compared the ratio of low- and high-avidity OVA tet^+ $CD4^+$ T cells, we consistently found in draining PLNs relatively more low-avidity T cells participating in the immune response in $TP^{-/-}$ mice compared with WT mice, despite comparable TCR expression levels (Fig. 1, C and D). A recent study has implicated neutrophil-derived TXA2 in the control of T cell responses (Yang and Unanue, 2013). We therefore performed OVA/CFA immunization in neutrophil-depleted WT and $TP^{-/-}$ mice. Similar to nondepleted mice, TP deficiency resulted in increased expansion of low-avidity $CD4^+$ T cells in PLNs (Fig. 1 E). To rule out an influence of different TCR repertoires in WT and $TP^{-/-}$ mice on expansion of low- and high-avidity $CD4^+$ T cells, we analyzed their ratio in control versus TP antagonist GR32191B-treated WT mice after s.c. OVA/CFA immunization. Again, we observed a skewing of the adaptive immune response toward low-avidity $CD4^+$ T cells in reactive GR32191B-treated WT PLNs as compared with controls (Fig. 1 F). In two independent experiments, the ratio of low- vs. high-avidity $CD4^+$ T cells from GR32191B-treated mice was increased by >30%.

To examine the relevance of TP-dependent tonic signaling in an infection model, we infected WT and $TP^{-/-}$ mice with lymphocytic choriomeningitis virus (LCMV) Armstrong strain. During LCMV Armstrong infection, we observed a nonsignificant tendency for increased expansion of $gp_{66\text{-}77}$ tet^+ $CD4^+$ T cells in $TP^{-/-}$ as compared with WT spleens ($8.8 \pm 3.3\%$ in WT vs. $14.8 \pm 9.1\%$ in $TP^{-/-}$ mice; mean $\pm$ SD), whereas no tet^+ $CD4^+$ T cells were observed in PLNs (unpublished data). Among the $gp_{66\text{-}77}$ tet^+ populations, the ratio of low- to high-avidity T cells was strongly skewed to the former in $TP^{-/-}$ mice (Fig. 1, G–I; and Fig. S1 C), despite comparable $CD4^+$ $FoxP3^+$ T reg cell percentages (not depicted). Collectively, the results obtained in sterile and infectious inflammation models suggest that absence of TP shapes the differential expansion of low- versus high-avidity T cells in a polyclonal repertoire.

Published December 8, 2014

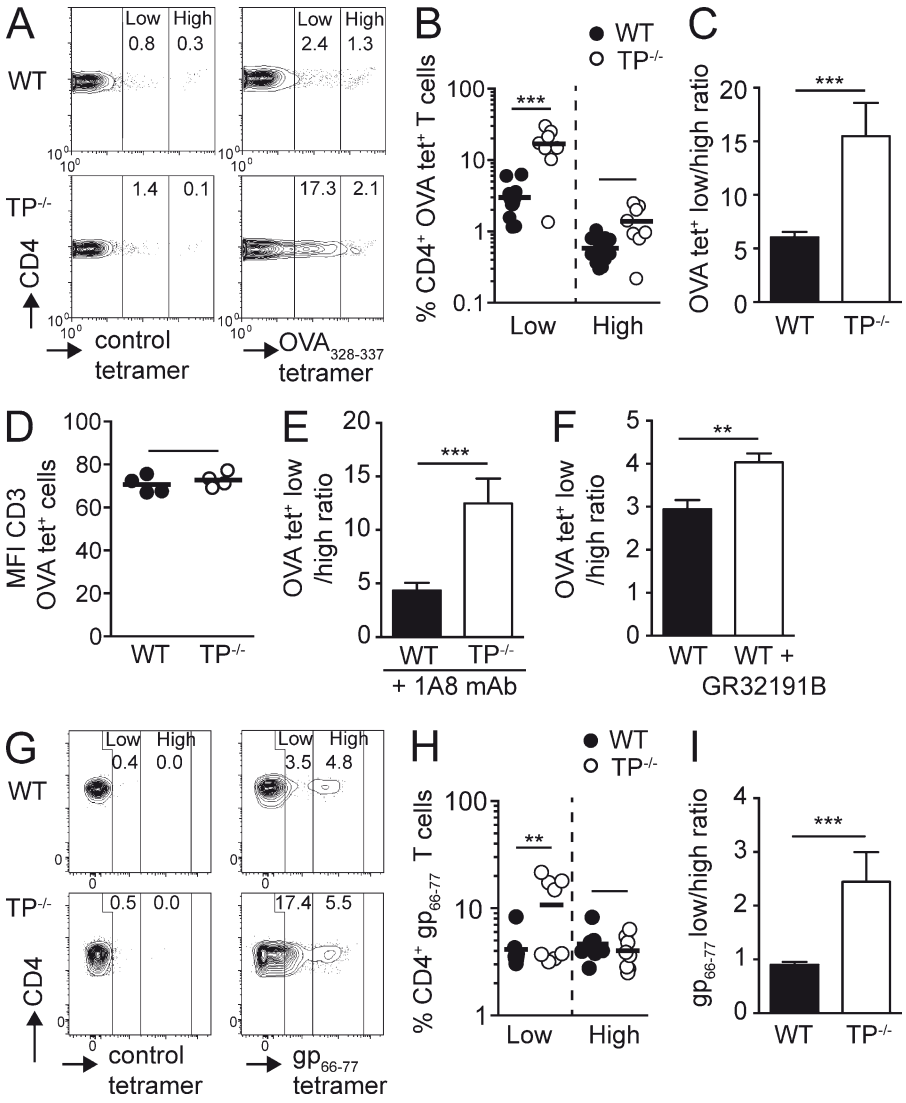

Figure 1. Absent TP signaling results in enhanced expansion of low-avidity CD4+ T cells during inflammation. (A–D) WT and $TP^{-/-}$ mice were immunized with OVA/CFA, and OVA-specific $CD4^+$ T cells in the draining peripheral LNs (PLNs) were analyzed on day 8 by tetramer staining. (A) Representative flow cytometry plots of polyclonal WT versus $TP^{-/-}$ $CD4^+$ T cells after gating on $CD4^+$ T cells and staining with control or OVA-specific tetramers. Numbers indicate percentage of $CD4^+$ T cells in low and high tet^+ gates. (B) Percentages of low and high OVA tet^+ $CD4^+$ T cells. (C) Ratio of low versus high OVA tet^+ $CD4^+$ T cells. (D) MFI of CD3 expression on OVA tet^+ WT and $TP^{-/-}$ T cells. (E and F) Mice were immunized as in A–D. Neutrophils were depleted by injecting anti-Ly6G antibody (1A8) on day −1 (E) or mice were treated with a selective thromboxane receptor antagonist (GR32191B) for 9 d starting 1 d before immunization (F). Ratio of low versus high OVA tet^+ $CD4^+$ T cells in draining PLNs at day 8 are shown. (G–I) WT and $TP^{-/-}$ were infected with LCMV Armstrong, and $CD4^+$ T cells in spleen were analyzed on day 8. (G) Representative flow cytometry plots of control and gp66-77 tet^+ $CD4^+$ T cells. Numbers indicate percentage of $7AAD^-$ $CD4^+$ T cells in low and high tet^+ gates. (H) Percentages of low versus high gp66-77 tet^+ $CD4^+$ T cells. (I) Ratio of low versus high gp66-77 tet^+ $CD4^+$ T cells. Data in B, C, and E are pooled from two independent experiments with a total of 4–7 mice per condition and combined staining of each sample with two different OVA tetramers, whereas D and F show representative data from one of two independent experiments with comparable results (3–4 mice/group). Data in G–I are pooled from two independent experiments with a total of 8 mice/group. Data in B and H were analyzed using ANOVA with Sidak's post-test, whereas C–F and I were analyzed using the Mann-Whitney test and are shown ±SEM. **, $P < 0.01$; ***, $P < 0.001$.

TP expression on naive OT-II $CD4^+$ T cells impairs in vivo interactions with DCs bearing low amounts or weak agonist pMHC complexes

The data obtained in our inflammation models prompted us to examine how TP influenced dynamic $CD4^+$ T cell–DC interactions in vivo. We therefore generated $TP^{-/-}$ OT-II $CD4^+$ T cells recognizing the $OVA_{323-339}$ peptide. Despite high expression of TP in thymocytes, $TP^{-/-}$ OT-II $CD4^+$ T cells displayed a bona fide naive phenotype characterized by high L-selectin/low CD44 expression and CD3 levels similar to WT OT-II $CD4^+$ T cells (unpublished data). Furthermore, WT and $TP^{-/-}$ OT-II $CD4^+$ T cells formed comparable in vitro immunological synapses (IS) defined by LFA-1 and PKCθ translocation to $OVA_{323-339}$-pulsed DCs and showed, in the absence of TP agonist I-BOP, similar proliferation and activation marker up-regulation after in vitro stimulation (unpublished data). Using these cells as tools in combination with DCs pulsed with varying OVA peptide concentrations, we performed 2PM of draining PLNs to directly investigate the effect of TXA2-TP signaling during initial T cell–DC interactions in vivo. As reported for T cell migration in explanted PLNs (Huang et al., 2007), lack of TP did not influence the speed, directionality, and motility coefficient (MC) of naive T cells as compared with WT T cells in nonreactive PLNs (Fig. 2 A and not depicted), presumably owing to low TXA2 levels in steady state. In contrast, activated DCs pulsed with 0.1 μM $OVA_{323-339}$ induced a significantly stronger deceleration of $TP^{-/-}$ OT-II $CD4^+$ T cell speeds as compared

Published December 8, 2014

with WT OT-II CD4+ T cells, accompanied by an increase of the arrest coefficient and a lower MC (Fig. 2, B and C; and Video 1). This speed difference disappeared when we examined T cell motility in the presence of DCs pulsed with 10 µM OVA peptide, although TP$^{-/-}$ OT-II CD4+ T cells still showed an increased arrest coefficient as compared with WT OT-II CD4+ T cells (Fig. 2, B and C; Video 2).

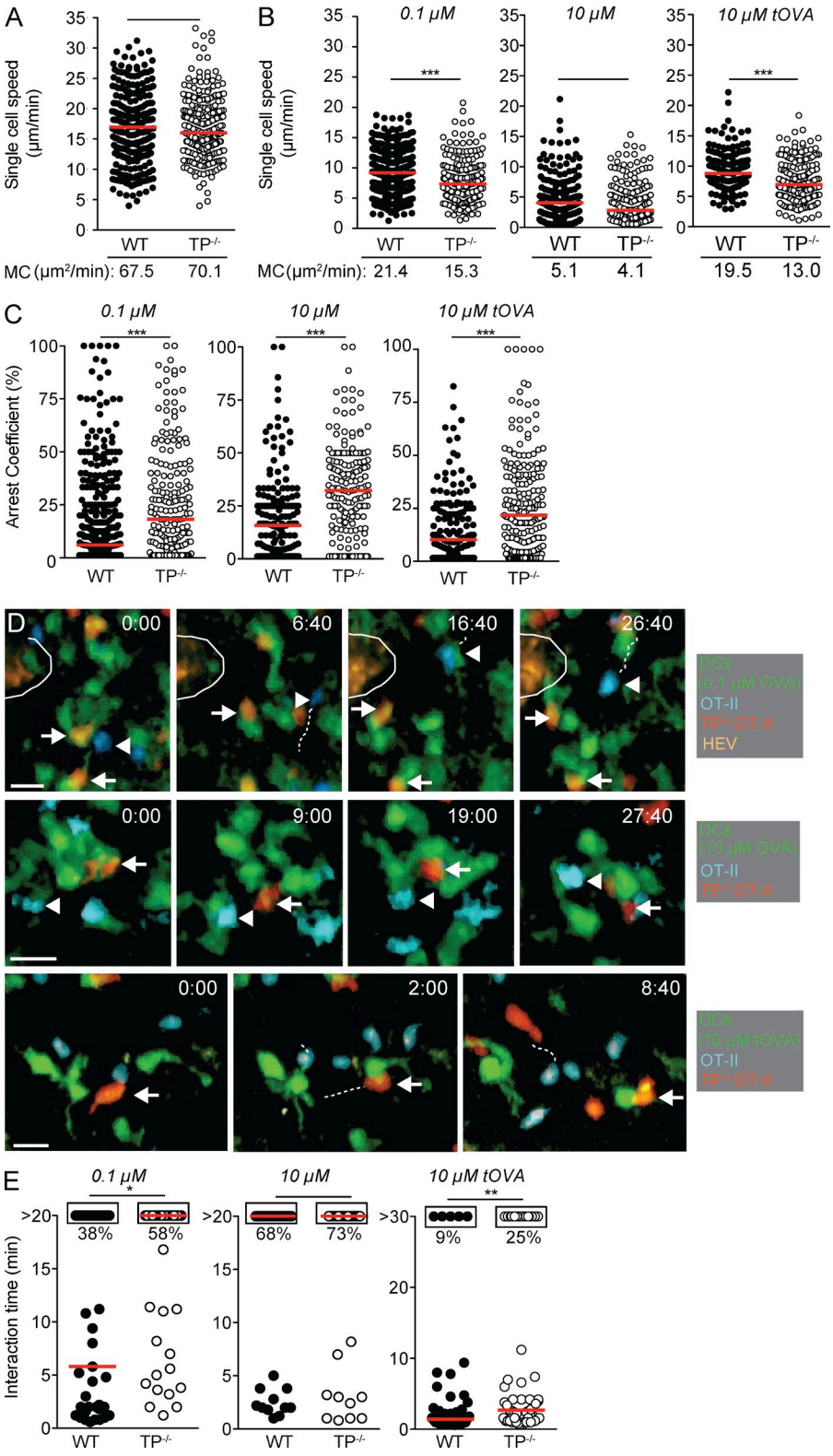

Figure 2. Intravital imaging of WT versus TP$^{-/-}$ OT-II CD4+ T cell interactions with pMHC-loaded DCs. (A–E) Polyclonal WT and TP$^{-/-}$ T cells were adoptively transferred in the absence of s.c. injected DCs (A) or WT and TP$^{-/-}$ OT-II CD4+ T cells were transferred in presence of DCs pulsed with indicated $OVA_{323-339}$ or turkey (t)$OVA_{324-340}$ (B–E). Single cell speeds and MC of adoptively transferred cells (A and B), their arrest coefficient (C) and T cell–DC interaction times (E) were monitored by 2PM imaging. D shows representative 2PM images of DC interactions with WT (arrowheads) and TP$^{-/-}$ OT-II CD4+ T cells (arrows). An encircled HEV is seen in the top row. Time is shown in minutes and seconds. Bar, 10 µm. Each dot represents one track (A–C) or interaction (E). Data in A–C and E are pooled from at least two independent experiments and were analyzed by Mann-Whitney test. Red bars indicate median. *, P < 0.05; **, P < 0.01; ***, P < 0.001.

Published December 8, 2014

When we analyzed the duration of T cell–DC contacts, we observed that WT OT-II CD4$^+$ T cells engaged in mostly short interactions with DCs pulsed with 0.1 µM $OVA_{323-339}$, with only 38% of observed interactions lasting >20 min (Fig. 2, D and E; and Video 3). In contrast, TP$^{-/-}$ OT-II CD4$^+$ T cells engaged longer with 0.1 µM $OVA_{323-339}$–pulsed DCs, with 58% of all observed interactions lasting throughout the observation period ($P < 0.05$). This difference was not observed when we quantified contact duration of WT and TP$^{-/-}$ OT-II CD4$^+$ T cells with DCs pulsed with 10 µM $OVA_{323-339}$. Under these conditions, stable interactions prevailed in both cell populations (68 vs. 73% for WT and TP$^{-/-}$ OT-II CD4$^+$ T cells, respectively; Fig. 2, D and E; and Video 4). At 18–24 h after transfer, we observed that both cell populations had detached from DCs and moved with similar migration speeds, suggesting that TP mostly controls T cell–DC interactions during the first hours of contact or during initial contact formation (unpublished data).

In addition to the abundance of cognate pMHC complexes, T cell–DC interactions are regulated by TCR-pMHC affinity. To examine this further, we used APL-pulsed DCs using 10 µM turkey OVA peptide ($tOVA_{324-340}$), which yields pMHC complexes with lower affinity for the OT-II TCR (Gollmer et al., 2009). In 2PM experiments, the majority of WT OT-II CD4$^+$ T cells interacted only briefly with $tOVA_{324-340}$-pulsed DCs and continued with high migration speeds and low arrest coefficient (Fig. 2, B–E; and Video 5). Absence of TP on OT-II CD4$^+$ T cells permitted these cells to interact significantly longer with tOVA-pulsed DCs (9 vs. 25% for WT and TP$^{-/-}$ OT-II CD4$^+$ T cells, respectively; $P < 0.01$), resulting in decreased migration speeds and increased arrest coefficients (Fig. 2, B–E; and Video 6). In sum, our 2PM imaging experiments suggest a role for TP in restraining naive CD4$^+$ T cell–DC interactions when cognate pMHC levels or TCR-pMHC affinities are low, in line with a function of cell-extrinsic tonic regulator. Tonic regulation prevents participation of naive lymphocytes in adaptive immune responses by raising the activation threshold, whereas T reg cells often act to dampen already activated T cells and are therefore considered reactive regulators in many cases (Germain, 2012).

Increased early OT-II CD4$^+$ T cell activation and T_{FH} generation in the absence of TP

We examined the consequences of increased duration of TP$^{-/-}$ OT-II CD4$^+$ T cell–DC interactions on effector differentiation. 24 h after transfer to recipient mice containing 0.1 µM $OVA_{323-339}$-pulsed DCs, TP$^{-/-}$ OT-II CD4$^+$ T cells showed increased expression of the early activation markers CD69 and CD25 as compared with WT OT-II CD4$^+$ T cells (Fig. 3, A–C). Higher CD69 and CD25 expression was also observed in TP$^{-/-}$ OT-II CD4$^+$ T cells after transfer with DCs pulsed with 10 µM $OVA_{323-339}$ (Fig. 3, A–C). This suggests that TP$^{-/-}$ OT-II CD4$^+$ T cells integrate signals more efficiently than TP-proficient cells over a wide range of pMHC densities. Notably, CD69 and CD25 expression levels of TP$^{-/-}$ OT-II CD4$^+$ T cells stimulated by 0.1 µM $OVA_{323-339}$-pulsed DCs were comparable to those of WT OT-II CD4$^+$ T cells stimulated by 10 µM $OVA_{323-339}$-pulsed DCs (Fig. 3 B), indicating that 100-fold lower pMHC levels were already sufficient to induce robust in vivo TP$^{-/-}$ OT-II CD4$^+$ T cell activation. Extrapolated to a polyclonal T cell population with variable TCR repertoire, the data obtained using a monoclonal TCR population suggest that the activation threshold for TP$^{-/-}$ CD4$^+$ T cells bearing low-avidity TCRs is substantially reduced as compared with WT CD4$^+$ T cells during inflammation. Given the abundance of low-avidity T cell clones during immune responses (Sabatino et al., 2011), this likely explains the substantial expansion of low-avidity CD4$^+$ T cells in the absence of TP signaling (Fig. 1).

High TCR binding strength results in the generation of follicular helper T cells (T_{FH}; Fazilleau et al., 2009), and TP$^{-/-}$ mice develop increased circulating antibody titers with age (Kabashima et al., 2003). We thus investigated whether the absence of TP influenced the generation of T_{FH} 8 d after OVA/CFA immunization in mice having received WT and TP$^{-/-}$ OT-II CD4$^+$ T cells. We found that the TP$^{-/-}$ OT-II CD4$^+$ T cells had expanded significantly more than WT CD4$^+$ T cells (Fig. 4, A and B; and Fig. S1 D), whereas both cell populations differentiated similarly into CXCR5^{high} PD-1^{high} T_{FH} (Fig. 4, C and D) and showed comparable expression of bcl-6 (Fig. 4 E), IL-21 (Fig. 4 F), and ICOS (not depicted). The similar percentage of T_{FH} generation in the absence of TP—despite increased expansion—likely reflects the constant pattern of effector cell differentiation inherent to OT-II TCR transgenic CD4$^+$ cells (Tubo et al., 2013). Germinal center (GC) B cells showed a parallel increased expansion in TP$^{-/-}$ as compared with WT OT-II CD4$^+$ T cell recipients (Fig. 4, G and H; and Fig. S1 E). Collectively, using a monoclonal CD4$^+$ T cell population, we identified a negative regulatory role of TP for weak T cell–DC interactions induced by limited amounts of cognate pMHC or APL presentation. The absence of TP on pMHC-specific transferred CD4$^+$ T cells sufficed to produce a substantial increase in T_{FH} and, as a consequence, GC B cells during inflammation.

Increased T_{FH} numbers in the absence of TP correlate with low-affinity IgG production

We investigated the functional consequences of TP$^{-/-}$ T_{FH} accumulation on the quality of ensuing IgG responses. We adoptively transferred WT or TP$^{-/-}$ OT-II CD4$^+$ T cells into SMARTA mice, in which the majority of CD4$^+$ T cells are specific for the $LCMVgp_{61-80}$ peptide and therefore unable to provide B cell help to other epitopes in the first 8 d after immunization (Oxenius et al., 1998; and unpublished data). After immunization with NP_{16}-OVA, we analyzed on day 8 serum titers of high- and low-affinity IgG by ELISA using NP_8- or NP_{41}-BSA-coated plates, respectively. We found that although both WT and TP$^{-/-}$ OT-II CD4$^+$ T cells were able to support similar titers of high-affinity IgG against NP_8-BSA, low-affinity anti–NP_{41}-BSA IgG production was substantially increased in SMARTA recipients transferred with TP$^{-/-}$ OT-II CD4$^+$ T cells (Fig. 5, A and B). Finally, we transferred OVA tet$^+$ CD4$^+$

Published December 8, 2014

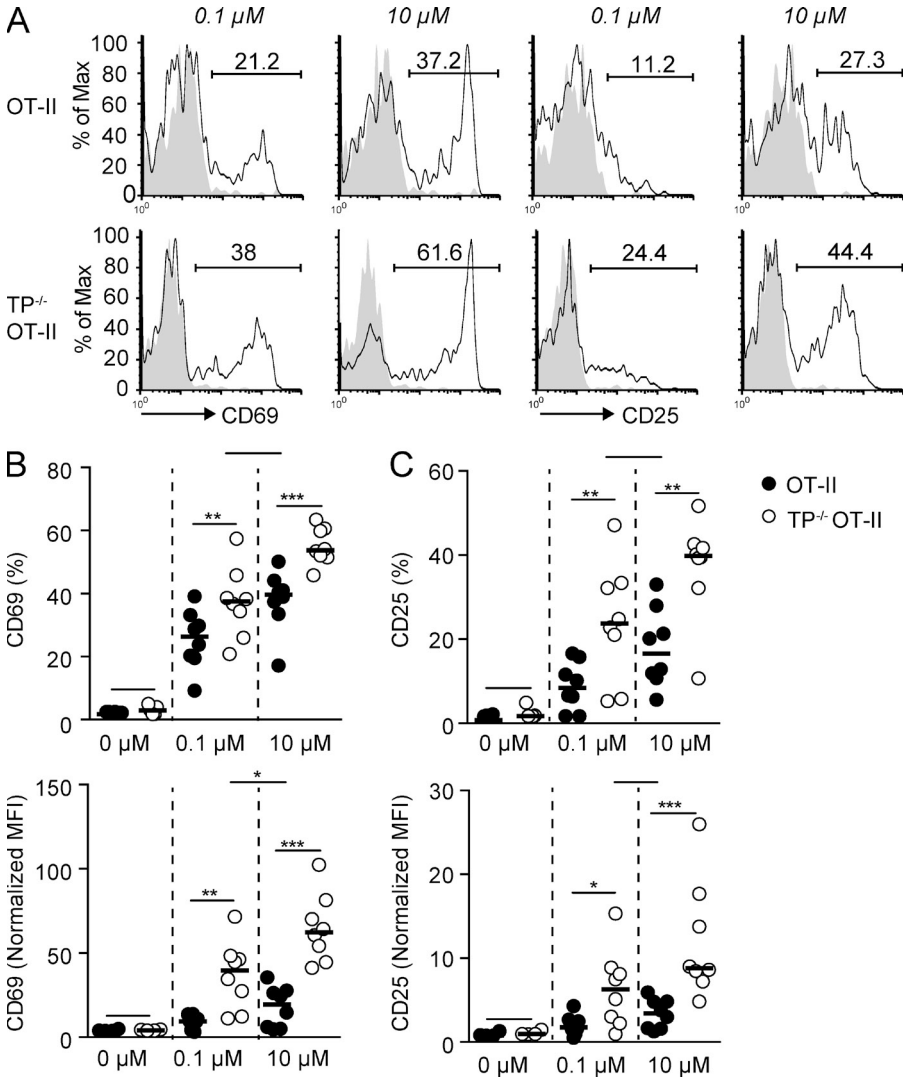

Figure 3. TP$^{-/-}$ OT-II CD4$^+$ T cells display increased activation marker expression as compared with WT OT-II CD4$^+$ T cells. (A-C) WT and TP$^{-/-}$ OT-II CD4$^+$ T cells were analyzed by flow cytometry 24 h after adoptive transfer in presence of DCs pulsed with low (0.1 μM) and high (10 μM) $OVA_{323-339}$ concentrations. A shows representative flow cytometry plots of CD25 and CD69 expression. Numbers indicate percent positive cells. Percentages and normalized MFI of CD69$^+$ (B) and CD25$^+$ (C) transferred WT and TP$^{-/-}$ OT-II CD4$^+$ T cells are shown. Each dot in B and C represents PLNs pooled from one mouse. Data are from 2–3 independent experiments with a total of 6–8 mice and analyzed using repeated measure ANOVA with Bonferroni post-test. Bars indicate mean. *, $P < 0.05$; **, $P < 0.01$; ***, $P < 0.001$.

T cells isolated from OVA-immunized WT and TP$^{-/-}$ mice into SMARTA mice and challenged the recipients with NP_{16}-OVA as above (Fig. S1 F). Again, we observed that mice transferred with TP$^{-/-}$ OVA tet$^+$ CD4$^+$ T cells showed skewing of the ensuing IgG response to low-affinity IgG compared with WT OVA tet$^+$ CD4$^+$ T cells, as reflected by a substantial increase in titers of NP_{41}- but not NP_8-BSA–binding IgG (Fig. 5 C). In sum, these data support a scenario where absence of TP leads to a significant rise in T_{FH} expansion, which has been associated with decreased quality of humoral responses (Pratama and Vinuesa, 2014). Alternatively, owing to their avid binding to cells bearing low pMHC levels, activated TP$^{-/-}$ CD4$^+$ T_{FH} cells, or their precursors, may provide help to B cells with low-affinity BCRs. To address this point experimentally, we used 2PM of HEL-OVA–draining PLNs to examine WT and TP$^{-/-}$ OT-II CD4$^+$ T cell interactions with HEL-specific MD4 or SW_{HEL} B cells at the border between T cell area and B cell follicles, where early CD4$^+$ T cell–B cell interactions (1–3 d after immunization) precede ensuing GC reactions (Vinuesa and Cyster, 2011). Although most T cell–B cell interactions were short-lived in these experiments (<5 min), we found occasional long interactions (>20 min) exclusively in the TP$^{-/-}$ CD4$^+$ T cell subset (unpublished data). However, because TP$^{-/-}$ OT-II CD4$^+$ T cells show increased expression of activation markers at early time points and the cognate pMHC density on individual B cells was unknown, these data remain difficult to interpret. Furthermore, 2PM experiments at later time points after immunization showed that TP antagonist GR32191B treatment did not reduce speeds of Ag-specific CD4$^+$ T cells migrating along FDCs (unpublished data). In line with this, TP expression decreases on effector T cells, including T_{FH}, and B cells do not express TXA2 synthase and do not secrete TXA2 (Immgen database; unpublished data; Kabashima et al., 2003). Recent evidence has uncovered that T_{FH} interact with GC B cells for only a short period of time, even when these cells present high levels of cognate pMHC (Shulman et al., 2014). It is therefore conceivable that excessive numbers of T_{FH} provide help to numerous GC B cells, which then drives production of low-affinity IgG. In line with this concept, T_{FH} help for cognate Ag-bearing GC B cells directly correlates with

Published December 8, 2014

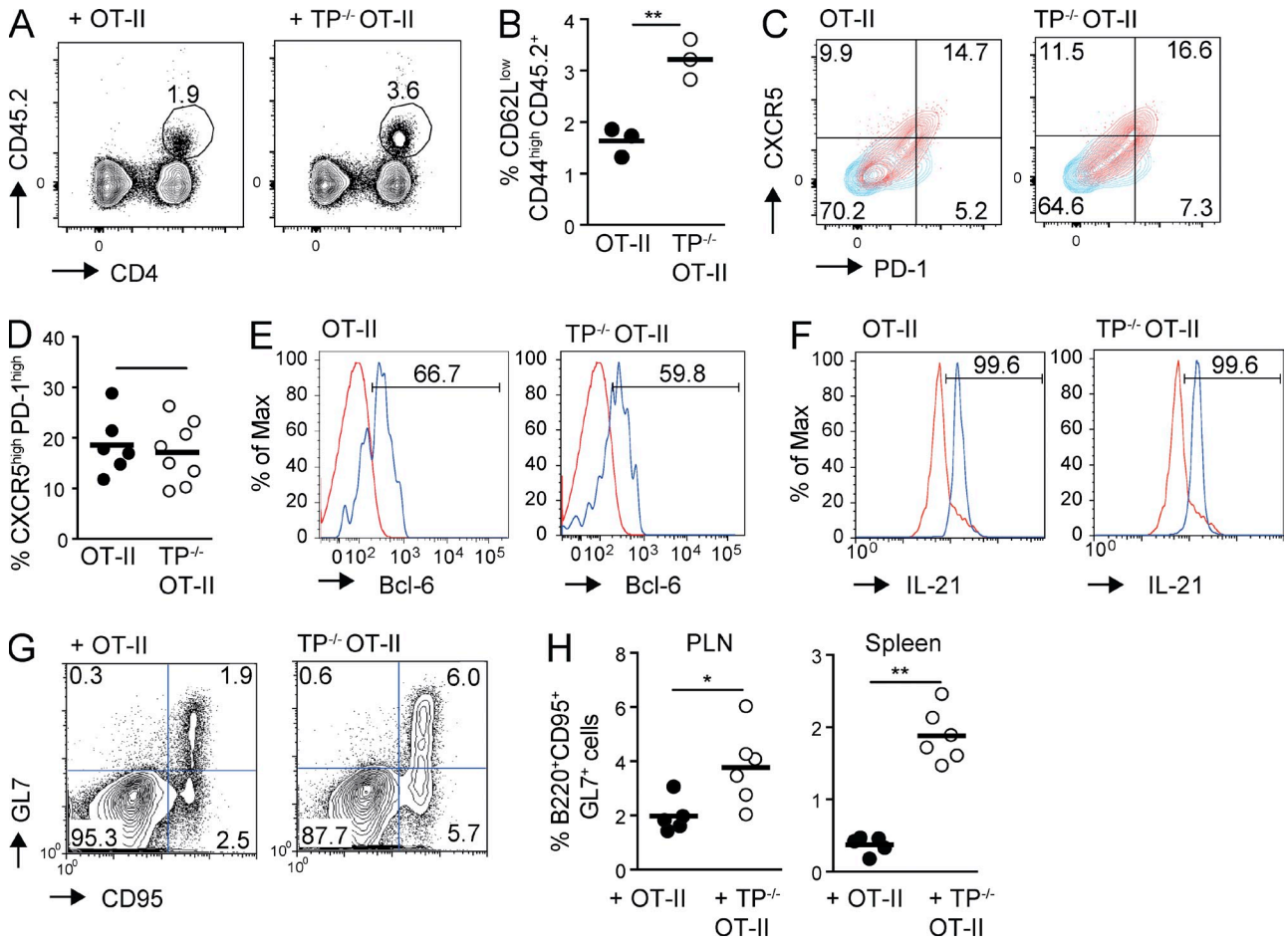

Figure 4. Increased numbers of T_{FH} in the absence of TP in OT-II CD4⁺ T cells. (A–H) WT and $TP^{-/-}$ OT-II CD4⁺ T cells were adoptively transferred separately (A–D and F–H) or combined (E) into CD45.1⁺ WT mice before immunization with OVA/CFA and analyzed on day 8 by flow cytometry. (A) Flow cytometry after pregating on $CD44^{high}$ $CD62L^{low}$ lymphocytes. Numbers indicate the percentage of circled CD45.2⁺ cells. (B) Percentage of adoptively transferred CD45.2⁺ T cells as pregated in A. (C) PD-1 and CXCR5 expression on transferred WT and $TP^{-/-}$ OT-II T cells (red), with numbers indicating percent per quadrant field. CD4⁺ T cells from a nonimmunized mouse serve as negative control (blue). (D) Percentage of PD-1^{high} $CXCR5^{high}$ CD45.2⁺ WT or $TP^{-/-}$ OT-II CD4⁺ T cells on day 8 after OVA/CFA immunization. Shown is one of three experiments, pooling T_{FH} from spleens and PLNs of 3–4 mice on day 8 after OVA/CFA immunization. (E) Flow cytometric analysis of intracellular bcl-6 expression (blue) in PD-1^{high} $CXCR5^{high}$ WT or $TP^{-/-}$ OT-II CD4⁺ T cells on day 8 after OVA/CFA immunization. As negative control, we plotted the endogenous CD45.1⁺ CD4⁺ cell signal (red), which gave an overlapping labeling as the isotype control (not depicted). (F) Flow cytometric analysis of intracellular IL-21 expression (blue) in $CXCR5^{high}$ WT or $TP^{-/-}$ OT-II CD4⁺ T cells on day 8 after OVA/CFA immunization. As negative control, we plotted the CD45.1⁺ CD4⁺ cell signal from a nonimmunized mouse (red), which gave an overlapping labeling as the isotype control (not depicted). (G) Flow cytometry plots of B220⁺ cells containing GL-7⁺ CD95⁺ GC B cells in WT or $TP^{-/-}$ OT-II T cell recipient mice on day 8 after OVA/CFA immunization with numbers indicating percent per quadrant field. (H) Percentage of GC B cells in WT or $TP^{-/-}$ OT-II T cell recipient mice 8 d after OVA/CFA immunization in PLNs and spleen. Each dot represents one mouse. Data are representative of three (A–F) or pooled from two (H) independent experiments with a total of 9–10 and 5–6 mice, respectively, and analyzed using Mann-Whitney test (B, D, and H). Bars indicate mean. *, $P < 0.05$; **, $P < 0.01$.

their expansion (Shulman et al., 2013; Gitlin et al., 2014) and unrestrained T_{FH} numbers are associated with autoimmunity and self-reactive B cells (Pratama and Vinuesa, 2014). This is likely to contribute to the development of lymphoid hyperplasia in older $TP^{-/-}$ mice (Kabashima et al., 2003), perhaps owing to excessive immune reactions to commensals in line with our observation of increased MLN size in these mice.

Immunoregulatory mechanisms need to be carefully balanced to simultaneously allow for a forceful adaptive immune response against pathogens to develop, while protecting the host from autoreactive T cells. How such a balance is achieved is not completely understood to date. Although immunosuppressive mechanisms have often been considered to generally hamper immune responses, Pace et al. (2012) have uncovered improved CD8⁺ T cell avidity in the presence of T reg cells. Similarly, we report that absence of TP increased the numbers of low-avidity CD4⁺ T cell clones transiting from kynapse- to synapse-like interactions with DCs (Bousso, 2008). In contrast to T reg cells or stromal cell–derived nitric oxide (Lukacs-Kornek et al., 2011), which typically function

Published December 8, 2014

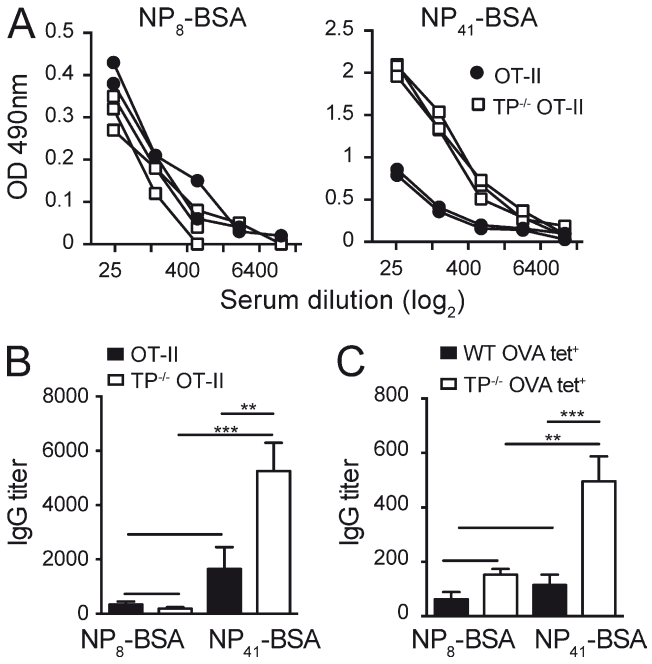

Figure 5. TP$^{-/-}$ CD4$^+$ T cells preferentially support low-avidity IgG responses. WT or TP$^{-/-}$ OT-II CD4$^+$ T cells (A and B) or OVA-tet$^+$ WT or TP$^{-/-}$ CD4$^+$ T cells (C) were adoptively transferred into SMARTA recipients before immunization with NP_{16}-OVA/CFA. On day 8 after infection, serum was isolated and IgG titers against NP_8-BSA and NP_{41}-BSA were measured in limited dilution assays. (A) Each line presents a dilution series of serum isolated from an individual mouse. (B) IgG titers to NP_8- and NP_{41}-BSA after transfer of WT or TP$^{-/-}$ OT-II CD4$^+$ T cells. (C) IgG titers to NP_8- and NP_{41}-BSA after transfer of OVA-tet$^+$ WT or TP$^{-/-}$ CD4$^+$ T cells. Data in B and C are pooled from two independent experiments with 4–5 mice/group and analyzed by ANOVA with Sidak's multiple comparison test. **, $P < 0.01$; ***, $P < 0.001$.

to suppress immune responses after their onset and act as reactive regulators (Germain, 2012), TP operates as tonic regulator to prevent the entry of poorly reactive naive CD4$^+$ T cells into a developing immune response. Our 2PM data revealed that TP-mediated disruption of T cell–DC interactions was gradually overcome by increasing pMHC levels on presenting DCs. In line with this observation, we found similar expansion of WT and TP$^{-/-}$ OT-II CD4$^+$ T_{FH} when we challenged mice with 10-fold higher OVA levels (unpublished data). Furthermore, infection with the LCMV clone 13, which leads to generalized infection and high antigen abundance until day 30 (Oldstone, 2009) resulted in comparable ratios of low- and high-avidity CD4$^+$ T cells in WT and TP$^{-/-}$ mice (unpublished data). An interesting aspect is that TXA2 levels are only increased in lymphoid tissue during inflammation (Moore et al., 1989), when DCs express high levels of co-stimulatory molecules. This suggests that reactive PLNs have developed specific mechanisms to avoid low-avidity bystander activation without affecting peripheral tolerance education of autoreactive T cells in noninflamed PLNs. The short half-life (<30 s) of TXA2, presumably produced by DCs, neutrophils, and macrophages, makes a paracrine action mode likely and provides the adaptive immune system with an additional layer of quality control. TXA2-induced chemokinesis and disruption of T cell–DC interactions is likely transmitted by Gα12/13-triggered activation of the Rho guanine exchange factor (GEF) lsc (Harenberg et al., 2005). The resulting rise of Rho-GTP then acts on mDia1 to induce cytoskeletal changes and chemokinesis (Sakata et al., 2007). In line with this hypothesis, we found that I-BOP–induced F-actin formation occurred independently of the Rac GEF DOCK2 (unpublished data), which is critical for actin cytoskeletal attachment of key proteins during IS formation (Sanui et al., 2003; Le Floc'h et al., 2013). An attractive model is therefore that the balance between DOCK2-Rac–driven IS assembly and TP-Rho–mediated disruptive chemokinesis determines successful activation of naive CD4$^+$ T cells in reactive PLNs.

In sum, our data help to understand how TP-TXA2 signaling contributes to the generation of high avidity CD4$^+$ T cell responses, and subsequent high affinity antibody production. Similar to T reg cell–mediated CD8$^+$ T cell avidity control (Pace et al., 2012), this mechanism involves preventing low-avidity T cell–DC interactions. Effector–memory T cells and T reg cell subsets decrease TP expression (Kabashima et al., 2003), which may contribute to their increased sensitivity to low pMHC levels on DCs.

MATERIALS AND METHODS

Mice. 4–6-wk-old male C57BL/6 mice were purchased from Janvier (AD Horst). LCMV gp61-80–specific Tg(TcrLCMV)Aox ("SMARTA"), C57BL/6-Tg(CAG-EGFP)131Osb/LeySopJ ("Ubi-GFP"), Tg(IghelMD4)4Ccg BCR-transgenic "MD4" (provided by E. Jacque, National institute for Medical Research, London, UK), C57BL/6-Tg(IgkHyHEL10)1Rbr ("SW_{HEL}"; provided by B. Stolp, University of Heidelberg, Germany), and TP$^{-/-}$ mice on a C57BL/6 background backcrossed to OT-II TCR transgenic mice specific for chicken OVA amino acids 323–339 were bred in the DKF animal facility in Bern. Animal work has been approved by the Cantonal Committee for Animal Experimentation and conducted according to federal and cantonal guidelines. Infection experiments were performed in accordance with federal and cantonal guidelines under permission numbers SG13/06 after review and approval by the Cantonal Veterinary Office (St. Gallen, Switzerland).

TP antagonist treatment and tetramer staining after OVA-CFA immunization. WT or TP$^{-/-}$ mice were immunized with chicken OVA/CFA emulsion (1 mg/ml; Sigma-Aldrich) injected s.c. in a volume of 30 µl/site in five points closed to inguinal, brachial, and cervical PLNs. In some experiments, WT mice were treated with a selective thromboxane receptor antagonist, GR32191B (Vapiprost, Sigma-Aldrich), in drinking water for 9 d, starting 1 d before OVA-CFA immunization, at a dose of 1 mg/kg/d. Mice were killed after 8 d, as described above, and tetramer staining was performed using the following tetramers (produced by National Institutes of Health Tetramer Core Facility, Atlanta, GA), diluted 1:10, for 2 h at 37°C: PVSKMRMATPLLMQA-PE-control (human $CLIP_{103-117}$), HAA-HAEINEA-PE-chicken $OVA_{328-337}$ (tetramer 1), IINFEKLTEWTSSNV-MEER-PE-chicken $OVA_{259-277}$ (tetramer 2), and AAHAEINEA-PE chicken $OVA_{329-337}$ (tetramer 3). All three OVA tetramers gave comparable results in flow cytometry.

Neutrophils were depleted by administration of the Ly6G-specific 1A8 mAb as previously described (Yang and Unanue, 2013), starting on day −1 before immunization and reinjected every 2 d. An isotype-matched mAb (2A3) was used as control. Depletion was verified by flow cytometry.

Published December 8, 2014

LCMV infection and flow cytometry analysis. LCMV strains Armstrong and Clone 13 were propagated on L929 cells and titrated by focus-forming assay on MC57 cells. Mice were infected i.v. with 10^3 PFU LCMV Armstrong or 10^7 PFU LCMV Clone 13. For flow cytometry, mice were sacrificed on day 8 after injection and single-cell suspensions from spleen and inguinal LNs were prepared by mechanical disruption of the organs. Analysis of LCMV-specific $CD8^+$ T cells was performed using PE-conjugated tetramers against LCMV gp_{33-41} and for $CD4^+$ T cell responses gp_{66-77}. We used as negative control the LCMV gp $precursor_{6-20}$ tetramer. MHC class II tetramer staining was performed for 90 min at 37°C. For surface staining, allophycocyanin-labeled anti-CD4 (BD) was used. Surface staining was performed by incubating samples at 4°C for 20 min 7-Aminoactinomycin D (EMD Millipore) was used to discriminate dead cells in flow cytometric analysis. Foxp3 staining was performed with the mouse regulatory T cell staining kit (eBioscience) using the Foxp3 PE (FJK-16) mAb. Samples were analyzed by flow cytometry using FACSCalibur (BD), and data were analyzed using FlowJo software (Tree Star).

T cell purification. LNs and spleens from WT or $TP^{-/-}$ mice were pooled and homogenized using a 70-µm cell strainer. Red blood cells were lysed in 1 ml of a Tris-HCL pH 7.5/0.83% ammonium-chloride buffer for 3 min. After washing in CM-R, a medium containing RPMI-1640 supplemented with 10% FCS, 100 U/ml penicillin, 100 U/ml streptomycin, 100 mM sodium pyruvate, L-glutamine, and nonessential amino acids (NEAAs), we used EasySep Mouse T cell Negative Selection kit or Mouse $CD4^+$ T cell enrichment kit as described in the manufacturer's instructions (STEMCELL Technologies). Total or $CD4^+$ T cells were negatively isolated in a magnetic holder. $CD4^+$ T cell purities were typically >95%.

DC culture and peptide pulsing. BM cell suspensions from Ubi-GFP mice were obtained by centrifugation (4,000 rpm, 4 min) of femurs and tibiae. BM cells were incubated in 20 ml cultures containing 18 ml CM-R and 2 ml SP-20 supernatant containing Flt3L for 6 to 9 d until activation with 1 µg/ml LPS (Sigma-Aldrich) for 24 h and pulsing with OVA peptides for 1 h at 37°C. Chicken $OVA_{323-339}$ (ISQAVHAAHAEINEAGR) and turkey $OVA_{324-340}$ (ISQAAHAAYAEIYEAGR) were obtained from Eurogentec.

2PM of popliteal PLNs. GFP-expressing DCs (2×10^6/mouse) were pulsed with indicated concentrations of chicken or turkey OVA peptide and injected s.c. in hindfoot of recipient mice 18 h before $CD4^+$ T cell transfer. Purified T cells were fluorescently labeled with 2.5 µM CMTMR or 20 µM CMAC for 15 min at 37°C, with dyes swapped between experiments. After washing, 5×10^6 labeled T cells were injected i.v. into sex-matched 5–10-wk-old anesthetized C57BL/6 recipient mice surgically prepared to expose the right popliteal PLN. 5 or 18–22 h after T cell transfer, 2PM imaging was performed using the TrimScope system equipped with a Olympus BX50WI fluorescence microscope and a 20× objective (NA 0.95; LaVision Biotec). 11–16 z-stacks (spacing 4 µm) of 250–300 × 250–300 µm x–y sections were acquired every 20 s for 20–30 min. Imaging was performed in the T cell area identified by the presence of HEVs labeled using Alexa Fluor 633–conjugated MECA-79 (15 µg/mouse). Sequences of image stacks were transformed into volume-rendered four-dimensional movies using Volocity software, which was also used for semiautomated tracking of cell motility in three dimensions. The average track speed, turning angles (defined as the angle between the two velocity vectors before and after a measurement time point) and motility coefficient were calculated from the x, y, and z coordinates of cell centroids. The arrest coefficient was determined as the percentage per track a cell moved slower than 4 µm/min.

For early T–B cell interaction analysis, fluorescently labeled WT and $TP^{-/-}$ OT-II T cells ($3–5 \times 10^6$ cells/mouse) were co-transferred i.v. with MD4 B cells or SW_{HEL} B cells ($3–5 \times 10^6$ cells/mouse) into C57BL/6 mice, which had been s.c. immunized 12 h before with 20 µl of a 1:1 mixture of CFA and chemically coupled HEL-OVA (final concentration 1.2 mg/ml) in the hock. To synchronize cell population behavior, we blocked further homing 4–10 h after transfer with 100 µg Mel-14/mouse. In some experiments, we injected PE-conjugated anti-CD35 mAb into footpads 18 h before imaging to label FDCs. 2PM of draining popliteal LNs was performed as above 42–48 h after cell transfer and T–B cell interactions were quantified using Volocity software. For analysis of OT-II $CD4^+$ T cell behavior in GC at later time points, we transferred 2.5×10^5 GFP-expressing OT-II $CD4^+$ T cells into recipient mice, which were immunized with 10 µl of a 3:1 mixture of OVA and the adjuvants Montanide ISA25 (final concentration 1.5 mg/ml) instead of CFA to avoid excessive foot swelling >3 d after immunization. On day 6 after immunization, we analyzed GFP^+ OT-II $CD4^+$ T cell migration in close apposition to $CD35^+$ FDCs using 2PM of the draining popliteal LNs in the presence or absence of the TP antagonist GR32191B.

Flow cytometry for activation markers. WT and $TP^{-/-}$ OT-II $CD4^+$ T cells were labeled with CFSE or e670 and analyzed 24 h after transfer into mice with pMHC-bearing DCs as described for 2PM experiments. Cell surface stainings were performed in staining buffer (PBS containing 1% FCS) for 30 min on ice in the dark, with the appropriate combinations of saturating concentrations of the following conjugated mAbs obtained from BioLegend: CD25 (3C7), CD69 (H1.2F3), and CD4 (GK1.5). Flow cytometry was performed on a FACSCalibur (BD) and FlowJo software (Tree Star) for analysis.

T_{FH} and GC B cell analysis in vivo. 5,000 CD45.1/.2^+ WT and CD45.2^+ $TP^{-/-}$ $CD4^+$ T cells were adoptively co-transferred into sex-matched CD45.1^+ C57BL/6 recipients. Alternatively, 5×10^3 CD45.2^+ WT or CD45.2^+ $TP^{-/-}$ $CD4^+$ T cells were separately transferred into sex-matched CD45.1^+ C57BL/6 recipients. The day after cell transfer, mice were immunized with chicken OVA/CFA emulsion (1 mg/ml; Sigma-Aldrich) injected s.c. in a volume of 30 µl/site in five points closed to inguinal, brachial and cervical PLNs. Recipients were killed after 8 d and cells from cervical, brachial, and inguinal nodes were pooled. Cell surface stainings were performed in staining buffer for 30 min, with the appropriate combinations of saturating concentrations of the following conjugated mAbs obtained from BD, eBioscience, or BioLegend: CD45.2 (104), CD45.1 (A20), GL-7 (GL-7), PD-1 (29F.1A12), ICOS (C398.4A), OX-40 (OX-86), Ly6C (HK1.4), PSGL-1, CD4 (RM4-5), CD45R (RA3-6B2), IgD (11-26c.2a), biotinylated CXCR5 (SPRCL5), followed by BV605-streptavidin, and biotinylated CD95, followed by BV421-streptavidin. In some experiments, cells were permeabilized using Cytofix/Cytoperm solution (BD) for staining with anti–IL-21 mAb (BL25168; BioLegend) or permeabilized with FoxP3 buffer for bcl6 (K112-91; BD) or FoxP3 (FJK-16S; eBioscience) staining according to manufacturer's instructions to confirm that adoptively transferred OT-II $CD4^+$ T cells do not form follicular regulatory T cells (Linterman et al., 2011). Stained cells were analyzed with LSRII or FACSCalibur flow cytometer (BD). Diva software or CellQuest were used for data acquisition, FlowJo software (Tree Star) was used for data analysis.

IgG titration. WT and $TP^{-/-}$ mice were immunized with chicken OVA/CFA emulsion as above, followed by staining with OVA tetramer 2 and FITC-conjugated anti-CD4 mAb (1:15,000 dilution to avoid depletion after transfer). Low and high tet^+ populations were sorted on a FACSAria II Flow Cytometer (BD), and 5×10^3 tet^+ low WT or $TP^{-/-}$ $CD4^+$ T cells were separately transferred into sex-matched SMARTA recipients. Owing to low numbers of recovered cells, we did not perform adoptive transfer of OVA tet^+ high $CD4^+$ T cells. Alternatively, 5×10^3 OT-II WT or $TP^{-/-}$ $CD4^+$ T cells were separately transferred into sex-matched SMARTA recipients. The day after cell transfer, mice were immunized with NP_{16}-OVA/CFA emulsion (1 mg/ml; 30 µl in five s.c. sites; Biosearch Technologies, Inc.). Recipients were killed after 8 d and serum was collected for IgG titration. In in brief, Nunc 96-well plates were plated with NP_8- or NP_{41}-BSA (0.1 µg/well; Biosearch Technologies, Inc.) diluted in coating buffer (15 mM carbonate buffer, pH 9.6) overnight at 4°C. After washing with washing buffer (WB) PBS/0.05% Tween-20 (Sigma-Aldrich), plates were incubated with 300 µl WB/5% dry milk for 2 h at room temperature. Serum dilutions (100 µl/well in 1:5 steps) were added and the plates were incubated for 2 h

at 37°C. After washing with WB, biotinylated polyclonal goat anti–mouse IgG (10 ng/well; AbD Serotec) diluted in WB was added for 1 h at room temperature. Wells were washed and incubated for 1 h at room temperature with 100 µl streptavidin-HRP (AbD Serotec) diluted 1/1,000 in WB. Bound antibodies were detected using OPD substrate, and absorbance was read at a wavelength of 490 nm. Results were calculated as titer by interpolation of absorbance values at a fixed serum dilution into a linear regression analysis plotting. Owing to the high molar ratio of NP moieties to BSA in the NP_{41}-BSA coated plates, low- and high-affinity anti-NP mAbs can bind, whereas only high affinity anti-NP mAbs bind to NP_8-BSA–coated plates.

Statistical analysis. Data were analyzed with GraphPad Prism 6 using Mann-Whitney test or ANOVA-one way test followed by Bonferroni's or Sidak's multiple comparison test. P values >0.05 were considered not significant.

Online supplemental material. Videos 1–6 show the dynamic interactions of OT-II $CD4^+$ T cells with DCs pulsed with 0.1 µM OVA, 10 µM OVA, and 10 µM tOVA. Fig. S1 shows the gating strategies used for flow cytometric analysis. Online supplemental materials are available at http://www.jem.org/cgi/content/full/jem.20140137/DC1.

We thank Markus Ackerknecht for advice on experiments, Bettina Stolp for SW_{HEL} mice, Emilie Jacque for MD4 mice, Milan Kubicek for scripts, Kenji Kabashima for discussion, Sarah Henrickson and Ulrich H. von Andrian for MatLab scripts, and Marcus Thelen and Britta Engelhardt for continuous support. We acknowledge the support from the Flow Cytometry core unit at the Department for Clinical Research. All tetramers used were from the National Institutes of Health tetramer core facility.

This work was supported by SNF grant 31003A_135649 (to JVS), SNF Sinergia grant CRSII3_141918 (to BL and JVS), a Japanese-Swiss Science and Technology Program grant (to YF and JVS), the Italian Association for Cancer Research (AIRC), and the Bangerter Foundation (to FM).

The authors declare no competing financial interests.

Submitted: 22 January 2014
Accepted: 5 November 2014

REFERENCES

Bajénoff, M., and R.N. Germain. 2007. Seeing is believing: a focus on the contribution of microscopic imaging to our understanding of immune system function. *Eur. J. Immunol.* 37:S18–S33. http://dx.doi.org/10.1002/eji.200737663

Bousso, P. 2008. T-cell activation by dendritic cells in the lymph node: lessons from the movies. *Nat. Rev. Immunol.* 8:675–684. http://dx.doi.org/10.1038/nri2379

Cahalan, M.D., and I. Parker. 2006. Imaging the choreography of lymphocyte trafficking and the immune response. *Curr. Opin. Immunol.* 18:476–482. http://dx.doi.org/10.1016/j.coi.2006.05.013

Fazilleau, N., L.J. McHeyzer-Williams, H. Rosen, and M.G. McHeyzer-Williams. 2009. The function of follicular helper T cells is regulated by the strength of T cell antigen receptor binding. *Nat. Immunol.* 10:375–384. http://dx.doi.org/10.1038/ni.1704

Germain, R.N. 2012. Maintaining system homeostasis: the third law of Newtonian immunology. *Nat. Immunol.* 13:902–906. http://dx.doi.org/10.1038/ni.2404

Gitlin, A.D., Z. Shulman, and M.C. Nussenzweig. 2014. Clonal selection in the germinal centre by regulated proliferation and hypermutation. *Nature.* 509:637–640. http://dx.doi.org/10.1038/nature13300

Gollmer, K., F. Asperti-Boursin, Y. Tanaka, K. Okkenhaug, B. Vanhaesebroeck, J.R. Peterson, Y. Fukui, E. Donnadieu, and J.V. Stein. 2009. CCL21 mediates CD4+ T-cell costimulation via a DOCK2/Rac-dependent pathway. *Blood.* 114:580–588. http://dx.doi.org/10.1182/blood-2009-01-200923

Harenberg, A., I. Girkontaite, K. Giehl, and K.-D. Fischer. 2005. The Lsc RhoGEF mediates signaling from thromboxane A2 to actin polymerization and apoptosis in thymocytes. *Eur. J. Immunol.* 35:1977–1986. http://dx.doi.org/10.1002/eji.200425769

Henrickson, S.E., and U.H. von Andrian. 2007. Single-cell dynamics of T-cell priming. *Curr. Opin. Immunol.* 19:249–258. http://dx.doi.org/10.1016/j.coi.2007.04.013

Huang, J.H., L.I. Cárdenas-Navia, C.C. Caldwell, T.J. Plumb, C.G. Radu, P.N. Rocha, T. Wilder, J.S. Bromberg, B.N. Cronstein, M. Sitkovsky, et al. 2007. Requirements for T lymphocyte migration in explanted lymph nodes. *J. Immunol.* 178:7747–7755. http://dx.doi.org/10.4049/jimmunol.178.12.7747

Hugues, S., L. Fetler, L. Bonifaz, J. Helft, F. Amblard, and S. Amigorena. 2004. Distinct T cell dynamics in lymph nodes during the induction of tolerance and immunity. *Nat. Immunol.* 5:1235–1242. http://dx.doi.org/10.1038/ni1134

Kabashima, K., T. Murata, H. Tanaka, T. Matsuoka, D. Sakata, N. Yoshida, K. Katagiri, T. Kinashi, T. Tanaka, M. Miyasaka, et al. 2003. Thromboxane A2 modulates interaction of dendritic cells and T cells and regulates acquired immunity. *Nat. Immunol.* 4:694–701. http://dx.doi.org/10.1038/ni943

Le Floc'h, A., Y. Tanaka, N.S. Bantilan, G. Voisinne, G. Altan-Bonnet, Y. Fukui, and M. Huse. 2013. Annular PIP3 accumulation controls actin architecture and modulates cytotoxicity at the immunological synapse. *J. Exp. Med.* 210:2721–2737. http://dx.doi.org/10.1084/jem.20131324

Linterman, M.A., W. Pierson, S.K. Lee, A. Kallies, S. Kawamoto, T.F. Rayner, M. Srivastava, D.P. Divekar, L. Beaton, J.J. Hogan, et al. 2011. Foxp3+ follicular regulatory T cells control the germinal center response. *Nat. Med.* 17:975–982. http://dx.doi.org/10.1038/nm.2425

Lukacs-Kornek, V., D. Malhotra, A.L. Fletcher, S.E. Acton, K.G. Elpek, P. Tayalia, A.-R. Collier, and S.J. Turley. 2011. Regulated release of nitric oxide by nonhematopoietic stroma controls expansion of the activated T cell pool in lymph nodes. *Nat. Immunol.* 12:1096–1104. http://dx.doi.org/10.1038/ni.2112

Moore, T.C., C.H. Spruck, J.L. Lami, and S.I. Said. 1989. Prompt elevations of PGE2 and thromboxane A2 metabolites in peripheral node efferent lymph of sheep following drainage area immunization. *Immunopharmacology.* 17:73–80. http://dx.doi.org/10.1016/0162-3109(89)90052-0

Morris, G.P., and P.M. Allen. 2012. How the TCR balances sensitivity and specificity for the recognition of self and pathogens. *Nat. Immunol.* 13:121–128. http://dx.doi.org/10.1038/ni.2190

Oldstone, M.B.A. 2009. Anatomy of viral persistence. *PLoS Pathog.* 5:e1000523. http://dx.doi.org/10.1371/journal.ppat.1000523

Oxenius, A., M.F. Bachmann, R.M. Zinkernagel, and H. Hengartner. 1998. Virus-specific MHC-class II-restricted TCR-transgenic mice: effects on humoral and cellular immune responses after viral infection. *Eur. J. Immunol.* 28:390–400. http://dx.doi.org/10.1002/(SICI)1521-4141(199801)28:01<390::AID-IMMU390>3.0.CO;2-O

Pace, L., A. Tempez, C. Arnold-Schrauf, F. Lemaitre, P. Bousso, L. Fetler, T. Sparwasser, and S. Amigorena. 2012. Regulatory T cells increase the avidity of primary CD8+ T cell responses and promote memory. *Science.* 338:532–536. http://dx.doi.org/10.1126/science.1227049

Pratama, A., and C.G. Vinuesa. 2014. Control of TFH cell numbers: why and how? *Immunol. Cell Biol.* 92:40–48. http://dx.doi.org/10.1038/icb.2013.69

Rachmilewitz, J., and A. Lanzavecchia. 2002. A temporal and spatial summation model for T-cell activation: signal integration and antigen decoding. *Trends Immunol.* 23:592–595. http://dx.doi.org/10.1016/S1471-4906(02)02342-6

Sabatino, J.J. Jr., J. Huang, C. Zhu, and B.D. Evavold. 2011. High prevalence of low affinity peptide-MHC II tetramer-negative effectors during polyclonal CD4+ T cell responses. *J. Exp. Med.* 208:81–90. http://dx.doi.org/10.1084/jem.20101574

Sakata, D., H. Taniguchi, S. Yasuda, A. Adachi-Morishima, Y. Hamazaki, R. Nakayama, T. Miki, N. Minato, and S. Narumiya. 2007. Impaired T lymphocyte trafficking in mice deficient in an actin-nucleating protein, mDia1. *J. Exp. Med.* 204:2031–2038. http://dx.doi.org/10.1084/jem.20062647

Sanui, T., A. Inayoshi, M. Noda, E. Iwata, M. Oike, T. Sasazuki, and Y. Fukui. 2003. DOCK2 is essential for antigen-induced translocation of TCR and lipid rafts, but not PKC-theta and LFA-1, in T cells. *Immunity.* 19:119–129. http://dx.doi.org/10.1016/S1074-7613(03)00169-9

Shakhar, G., R.L. Lindquist, D. Skokos, D. Dudziak, J.H. Huang, M.C. Nussenzweig, and M.L. Dustin. 2005. Stable T cell-dendritic cell interactions precede the development of both tolerance and immunity in vivo. *Nat. Immunol.* 6:707–714. http://dx.doi.org/10.1038/ni1210

Shulman, Z., A.D. Gitlin, J.S. Weinstein, B. Lainez, E. Esplugues, R.A. Flavell, J.E. Craft, and M.C. Nussenzweig. 2014. Dynamic signaling by T follicular helper cells during germinal center B cell selection. *Science.* 345:1058–1062. http://dx.doi.org/10.1126/science.1257861

Shulman, Z., A.D. Gitlin, S. Targ, M. Jankovic, G. Pasqual, M.C. Nussenzweig, and G.D. Victora. 2013. T follicular helper cell dynamics in germinal centers. *Science.* 341:673–677. http://dx.doi.org/10.1126/science.1241680

Su, L.F., B.A. Kidd, A. Han, J.J. Kotzin, and M.M. Davis. 2013. Virus-specific CD4(+) memory-phenotype T cells are abundant in unexposed adults. *Immunity.* 38:373–383. http://dx.doi.org/10.1016/j.immuni.2012.10.021

Tadokoro, C.E., G. Shakhar, S. Shen, Y. Ding, A.C. Lino, A. Maraver, J.J. Lafaille, and M.L. Dustin. 2006. Regulatory T cells inhibit stable contacts between CD4+ T cells and dendritic cells in vivo. *J. Exp. Med.* 203:505–511. http://dx.doi.org/10.1084/jem.20050783

Tang, Q., J.Y. Adams, A.J. Tooley, M. Bi, B.T. Fife, P. Serra, P. Santamaria, R.M. Locksley, M.F. Krummel, and J.A. Bluestone. 2006. Visualizing regulatory T cell control of autoimmune responses in nonobese diabetic mice. *Nat. Immunol.* 7:83–92. http://dx.doi.org/10.1038/ni1289

Tubo, N.J., A.J. Pagán, J.J. Taylor, R.W. Nelson, J.L. Linehan, J.M. Ertelt, E.S. Huseby, S.S. Way, and M.K. Jenkins. 2013. Single naive CD4+ T cells from a diverse repertoire produce different effector cell types during infection. *Cell.* 153:785–796. http://dx.doi.org/10.1016/j.cell.2013.04.007

Vinuesa, C.G., and J.G. Cyster. 2011. How T cells earn the follicular rite of passage. *Immunity.* 35:671–680. http://dx.doi.org/10.1016/j.immuni.2011.11.001

Yang, C.-W., and E.R. Unanue. 2013. Neutrophils control the magnitude and spread of the immune response in a thromboxane A2-mediated process. *J. Exp. Med.* 210:375–387. http://dx.doi.org/10.1084/jem.20122183

SUPPLEMENTAL MATERIAL

Moalli et al., http://www.jem.org/cgi/content/full/jem.20140137/DC1

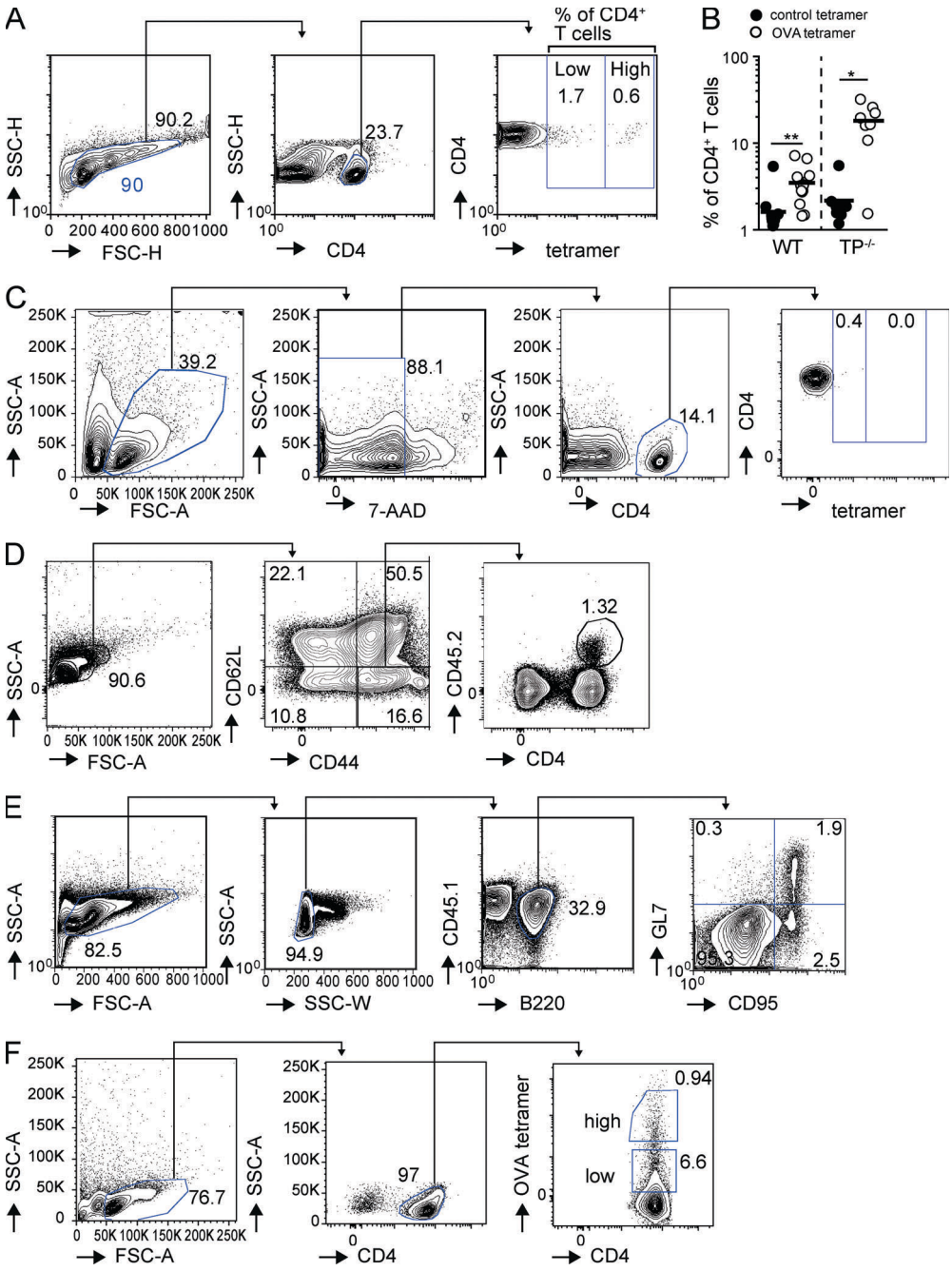

Figure S1. Gating strategies for flow cytometric analysis. (A) Gating strategy of OVA tet+ CD4+ T cells after OVA/CFA immunization. Numbers indicate percentages of gated populations. (B) Percentages of control and OVA tet+ CD4+ T cells in draining PLNs of WT and $TP^{-/-}$ mice. (C) Gating strategy for flow cytometric analysis of gp_{66-77} tet+ CD4+ T cells after LCMV Armstrong infections. (D) Gating strategy of adoptively transferred CD4+ $CD44^{high}$ $CD62^{low}$ CD45.2+ WT or $TP^{-/-}$ OT-II CD4+ T cells on day 8 after OVA/CFA immunization. (E) Gating strategy for flow cytometric analysis of germinal center B cells on day 8 after OVA/CFA immunization. (F) Sorting strategy by flow cytometry for low and high OVA tet+ CD4+ T cells on day 8 after OVA/CFA-immunization of WT and $TP^{-/-}$ mice. Numbers indicate percentages of gated populations. Owing to low numbers of recovered high OVA tet+ CD4+ T cells, we did not transfer these cells into SMARTA mice. Data in B are pooled from two independent experiments with 4–8 mice/group and analyzed using a Kruskal-Wallis test. *, $P < 0.05$; **, $P < 0.01$.

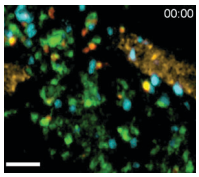

Video 1. 2PM image sequence showing WT (blue) and TP$^{-/-}$ (red) OT-II CD4$^+$ T cells and DCs (green) pulsed with 0.1 µM OVA. Selected WT and TP$^{-/-}$ OT-II CD4$^+$ T cells tracks are shown in blue and red, respectively. HEVs are labeled brown. Time is shown in minutes and seconds. Bar, 25 µm.

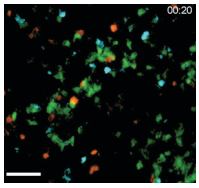

Video 2. 2PM image sequence showing WT (blue) and TP$^{-/-}$ (red) OT-II CD4$^+$ T cells and DCs (green) pulsed with 10 µM OVA. Selected WT and TP$^{-/-}$ OT-II CD4$^+$ T cells tracks are shown in blue and red, respectively. Time is shown in minutes and seconds. Bar, 30 µm.

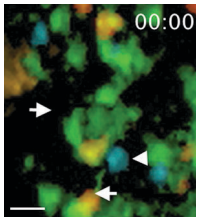

Video 3. 2PM image sequence showing WT (blue) and TP$^{-/-}$ (red) OT-II CD4$^+$ T cells interacting with DCs (green) pulsed with 0.1 µM OVA. Interactions with DCs are labeled with arrowheads for WT and arrows for TP$^{-/-}$ OT-II CD4$^+$ T cells, respectively. An HEV (brown) is seen in the top left corner. Time is shown in minutes and seconds. Bar, 15 µm.

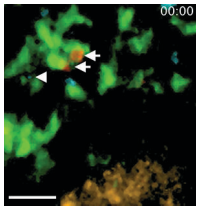

Video 4. 2PM image sequence showing WT (blue) and TP$^{-/-}$ (red) OT-II CD4$^+$ T cells interacting with DCs (green) pulsed with 10 µM OVA. Interactions are labeled as in Video 3. An HEV (brown) is seen in the bottom. Time is shown in minutes and seconds. Bar, 15 µm.

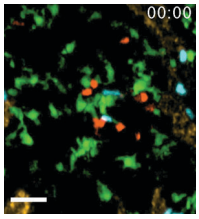

Video 5. 2PM image sequence showing WT (blue) and TP$^{-/-}$ (red) OT-II CD4$^+$ T cells and DCs (green) pulsed with 10 µM tOVA. Selected WT and TP$^{-/-}$ OT-II CD4$^+$ T cells tracks are shown in blue and red, respectively. HEVs are labeled brown. Time is shown in minutes and seconds. Bar, 30 µm.

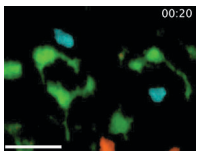

Video 6. 2PM image sequence showing WT (blue) and TP$^{-/-}$ (red) OT-II CD4$^+$ T cells interacting with DCs (green) pulsed with 10 µM tOVA. Interactions are labeled as in video 3. Time is shown in minutes and seconds. Bar, 10 µm.